Integrin-linked kinase regulates melanosome trafficking and melanin transfer in melanocytes

Melissa Crawford[a], Nancy Liu[a], Elahe Mahdipour[a,b], Kevin Barr[a], Bryan Heit[c], and Lina Dagnino[a,d,*]
[a]Department of Physiology and Pharmacology, Children's Health Research Institute and Lawson Health Research Institute, [c]Department of Microbiology and Immunology and Robarts Research Institute, and [d]Department of Oncology, University of Western Ontario, London, ON N6G 2C4, Canada; [b]Department of Medical Biotechnology and Nanotechnology, Mashhad University of Medical Sciences, Mashhad, Iran

ABSTRACT **Melanosomes are melanin-containing organelles that provide pigmentation and protection from solar UV radiation to the skin. In melanocytes, melanosomes mature and traffic to dendritic tips, where they are transferred to adjacent epidermal keratinocytes through pathways that involve microtubule networks and the actin cytoskeleton. However, the role of scaffold proteins in these processes is poorly understood. Integrin-linked kinase (ILK) is a scaffold protein that regulates microtubule stability and F-actin dynamics. Here we show that ILK is necessary for normal trafficking of melanosomes along microtubule tracks. In the absence of ILK, immature melanosomes are not retained in perinuclear regions, and mature melanosome trafficking along microtubule tracks is impaired. These deficits can be attenuated by microtubule stabilization. Microtubules are also necessary for the formation of dendrites in melanocytes, and *Ilk* inactivation reduces melanocyte dendricity. Activation of glycogen synthase kinase-3 (GSK-3) interferes with microtubule assembly. Significantly, inhibition of GSK-3 activity or exogenous expression of the GSK-3 substrate collapsin response mediator protein 2 (CRMP2) in ILK-deficient melanocytes restored dendricity. ILK is also required for normal melanin transfer, and GSK-3 inhibition in melanocytes partially restored melanin transfer to neighboring keratinocytes. Thus, our work shows that ILK is a central modulator of melanosome movements in primary epidermal melanocytes and identifies ILK and GSK-3 as important modulators of melanin transfer to keratinocytes, a key process for epidermal UV photoprotection.**

Monitoring Editor
Asma Nusrat
University of Michigan

Received: Sep 16, 2019
Revised: Jan 31, 2020
Accepted: Feb 4, 2020

INTRODUCTION

Pigmentation in the skin is achieved through sequential processes that involve synthesis of melanin in melanocytes, followed by its transfer to adjacent epidermal keratinocytes (Wu and Hammer, 2014). Melanin is synthesized and stored in melanosomes, lysosome-related organelles that first arise from endosomal vesicles generated in perinuclear regions (Raposo and Marks, 2007). As melanosomes mature, they synthesize melanin and increase their melanin content, undergo microtubule- and F-actin–dependent transport toward the cell periphery, and eventually become tethered to the plasma membrane. Stimulation of melanocytes by UV radiation and/or paracrine signals from keratinocytes and other cell types induces cytoskeletal reorganization, a process required for the formation of dendrites in which melanosomes accumulate (Evans *et al.*, 2014) The interaction of melanocyte dendritic tips with neighboring keratinocytes promotes transfer of melanosomes or melanosome cores in the only known example of intercellular organelle movements in vertebrates (Tadokoro *et al.*, 2016; Correia *et al.*, 2018). Alterations in melanocyte genes that encode proteins required for melanosome transport and distribution cause a multitude of pigmentary disorders (Yamaguchi and Hearing, 2014).

Integrin-liked kinase (ILK) is a ubiquitous adaptor protein with major regulatory roles in F-actin and microtubule cytoskeletal

This article was published online ahead of print in MBoC in Press (http://www.molbiolcell.org/cgi/doi/10.1091/mbc.E19-09-0510) on February 12, 2020.

The authors declare no conflict of interest.

Author contributions: M.C. and L.D. conceptualized the project; M.C., N.L., E.M., B.H., and L.D. carried out formal analysis; L.D. acquired funding; M.C., N.L., E.M., K.B., and L.D. investigated; M.C., E.M., and L.D. developed methodology; L.D. administered the project; L.D. provided resources; L.D. supervised; M.C., N.L., E.M., and L.D. provided validation; M.C., N.L., E.M., and L.D. visualized the results; M.C. wrote the original draft; L.D. reviewed and edited the manuscript.

*Address correspondence to: Lina Dagnino (ldagnino@uwo.ca).

Abbreviations used: CRMP2, collapsing response mediator protein 2; GFP, green fluorescent protein; GSK-3, glycogen synthase kinase-3; ILK, integrin-linked kinase; 4OHT, 4-hydroxytamoxifen.

remodeling (Wickstrom *et al.*, 2010; Jackson *et al.*, 2015; Vaynberg *et al.*, 2018). In neuroectoderm-derived cells, including melanocytes, oligodendrocytes, and Schwann cells, ILK is required for formation of cell extensions that fulfill critical functional roles. For example, inactivation of the *Ilk* gene in oligodendrocytes and in Schwann cells impairs their ability to extend processes to contact and allow interactions with neuronal axons, through mechanisms that involve deregulation of F-actin cytoskeletal dynamics (Pereira *et al.*, 2009; O'Meara *et al.*, 2013). ILK is required for the generation of cell protrusions involved in embryonic melanoblast migration and homing to the skin. In postnatal epidermal melanocytes, ILK also mediates formation and elongation of actin-rich dendrites in response to soluble factors or extracellular matrix substrates, through Rac1-dependent processes (Crawford *et al.*, 2019). Given that dendrite formation and cytoskeletal rearrangements are requisites for optimal melanin transfer, we investigated the role of ILK in modulation of melanosome movements. To this end, we assessed the consequences of conditional inactivation of *Ilk* in primary epidermal melanocytes for melanosome trafficking and the ability of these cells to transfer melanin to neighboring epidermal keratinocytes.

RESULTS

Altered melanosome dynamics in ILK^{KO} melanocytes

To investigate the role of ILK in melanosome trafficking, we isolated primary *Tyr::CreER^{T2};ROSA$^{mT/mG}$;Ilk$^{f/f}$* melanocytes and cultured them to >95% purity, as we previously described (Crawford *et al.*, 2017). In the absence of CreER^{T2} activation, these cells express a membrane-bound form of Tomato fluorescent protein (mTomato) (Crawford *et al.*, 2017). Treatment with 4OHT yields ILK-deficient cells that can be identified readily because they express a membrane-bound form of GFP, although mTomato fluorescence remains detectable in these cells up to 5–7 d after 4OHT administration (Supplemental Figure 1A; Crawford *et al.*, 2019). Under these conditions, the amount of melanin present in ILK^{KO} melanocytes is similar to that in ILK-expressing cells (Supplemental Figure 1B). We first acquired time-lapse bright-field videomicroscopy images of these cultures to examine the movement patterns of mature (stage III–IV), melanin-containing melanosomes, readily identified by the presence of dark melanin pigment using bright field microscopy. Within the melanocyte cell body, melanosomes travel bidirectionally along microtubule tracks, eventually reaching the tip of dendritic extensions, where they are transferred to cortical F-actin (reviewed in Van Gele *et al.*, 2009). In agreement with this concept, melanosomes moving in a linear manner toward the cell periphery or alongside dendrites were readily observed in ILK-expressing melanocytes (hereafter termed ILK^{+} cells; Figure 1A and Supplemental Movie 1). In contrast, melanosomes in ILK-deficient cells (hereafter termed ILK^{KO} melanocytes) appeared to move in a more rapid and random manner (Figure 1A and Supplemental Movie 2). Examination of trajectory plots revealed that melanosomes in ILK^{+} cells and ILK^{KO} cells displayed average speeds of 0.02 μm/s and 0.05 μm/s, respectively (Figure 1B). Similarly, we observed a significant difference in the mean distance traveled during a 10-min imaging period: ~17 μm in ILK^{+} and ~28 μm in ILK^{KO} cells (Figure 1B).

Analysis of melanosome movements uncovered a subset that exhibited restricted mobility and average velocity values (V_{avg}) ≤ 0.01 μm/s, proposed to represent melanosomal particles docked to microtubules (Bruder *et al.*, 2012). This subset was statistically similar in the two cell types, constituting ~34% and ~22% of all melanosomes analyzed in ILK^{+} and ILK^{KO} cells, respectively (Figure 1C). In ILK^{+} cells, about 50% of melanosomes moved mainly along linear *x–y* paths with V_{avg} values in the range 0.01–0.05 μm/s, which likely reflect active transport along microtubule tracks (Trinczek *et al.*, 1999). Loss of ILK expression significantly reduced this melanosome population, about twofold (Figure 1C). Finally, whereas only a small proportion of melanosomes with V_{avg} in the range of 0.01–0.05 μm/s exhibited oscillatory, nonlinear movements in ILK^{+} cells, about 50% of melanosomes in ILK^{KO} melanocytes displayed fast nonlinear movements. Indeed, a substantial fraction of these particles exhibited V_{avg} values ≥ 0.05 μm/s (Figure 1C).

We further investigated the displacement characteristics of the melanosomes. Migration index values, which provide a measure of the directness of melanosome trajectories, were greater in melanosomes from ILK^{+} cells (0.19 ± 0.04) than in those from ILK^{KO} melanocytes (0.09 ± 0.007; Figure 1D). Finally, we assessed processivity, defined as the ability of melanosomal particles to sustain movement in the same direction. The average processivity values in ILK^{+} cells were 4.32 ± 0.26, significantly higher than those in ILK^{KO} melanocytes (3.11 ± 0.07; Figure 1D). Together, these observations suggest that the absence of ILK possibly causes alterations in melanosome trafficking along cytoskeletal tracks.

Dispersion of stage I–II melanosomes in the absence of ILK

Melanosome biogenesis is integrated with endosomal pathways, but melanosomes are distinct from endosomal organelles (Gomez *et al.*, 2001; Jordens *et al.*, 2006; Hida *et al.*, 2011). Rab7 is required for early stages of melanosome formation. Indeed, Rab7 immunoreactivity specifically in melanocytes is for the most part associated with Stage I–II melanosomes, with small contributions from a subset of TYRP1-containing late endosomes (Gomez *et al.*, 2001; Jordens *et al.*, 2006; Hida *et al.*, 2011). Thus, we next investigated whether the absence of ILK is also associated with abnormalities in early-stage, amelanotic melanosomes, characterized by the presence of PMEL and Rab7. Stage I–II immature melanosomes associate with complexes containing Rab7 and dynein, which promotes transport toward the minus end of microtubules and perinuclear clustering of these vesicles around microtubule organizing centers (Jordens *et al.*, 2001). We observed that, in normal melanocytes, Rab7 immunoreactivity concentrated within a perinuclear belt region, with minimal presence in the cell periphery (Figure 2A). In contrast, Rab7-containing vesicles in ILK^{KO} melanocytes were dispersed throughout the cell, including regions within observable dendritic extensions present in these cells (Figure 2A). Quantification of Rab7-associated fluorescence revealed a ~50% greater contribution in regions outside the perinuclear belt in the absence of ILK (Figure 2B).

In melanocytes, Rab9a is necessary for normal pigmentation and for cargo delivery from late endosomes (Mahanty *et al.*, 2016). We investigated if ILK-deficient melanocytes exhibit abnormalities in the distribution of Rab9a-associated late endosomes. We observed Rab9a immunoreactivity in vesicles distributed throughout the cell, irrespective of the presence or absence of ILK (Figure 2D).

We also determined whether Rab7-positive vesicles colocalize with Rab9a immunoreactivity. To this end, we isolated melanocytes from *Ilk$^{f/f}$* mice, in which both *Ilk* alleles are flanked by loxP sites (Terpstra *et al.*, 2003), and transduced them with an adenovirus encoding GFP-tagged Cre recombinase (AdCre). This approach allowed us to better visualize Rab7 and Rab9a immunoreactivity in targeted cells, without mTomato-associated fluorescence. In these cells, ILK becomes undetectable 5 d after AdCre transduction (Supplemental Figure 2A; Crawford *et al.*, 2019). In agreement with their reported localization to endosomes and early melanosomes, respectively, Rab9a and Rab7 immunoreactivities were reciprocally exclusive in the majority of vesicles in nontransduced ILK-expressing

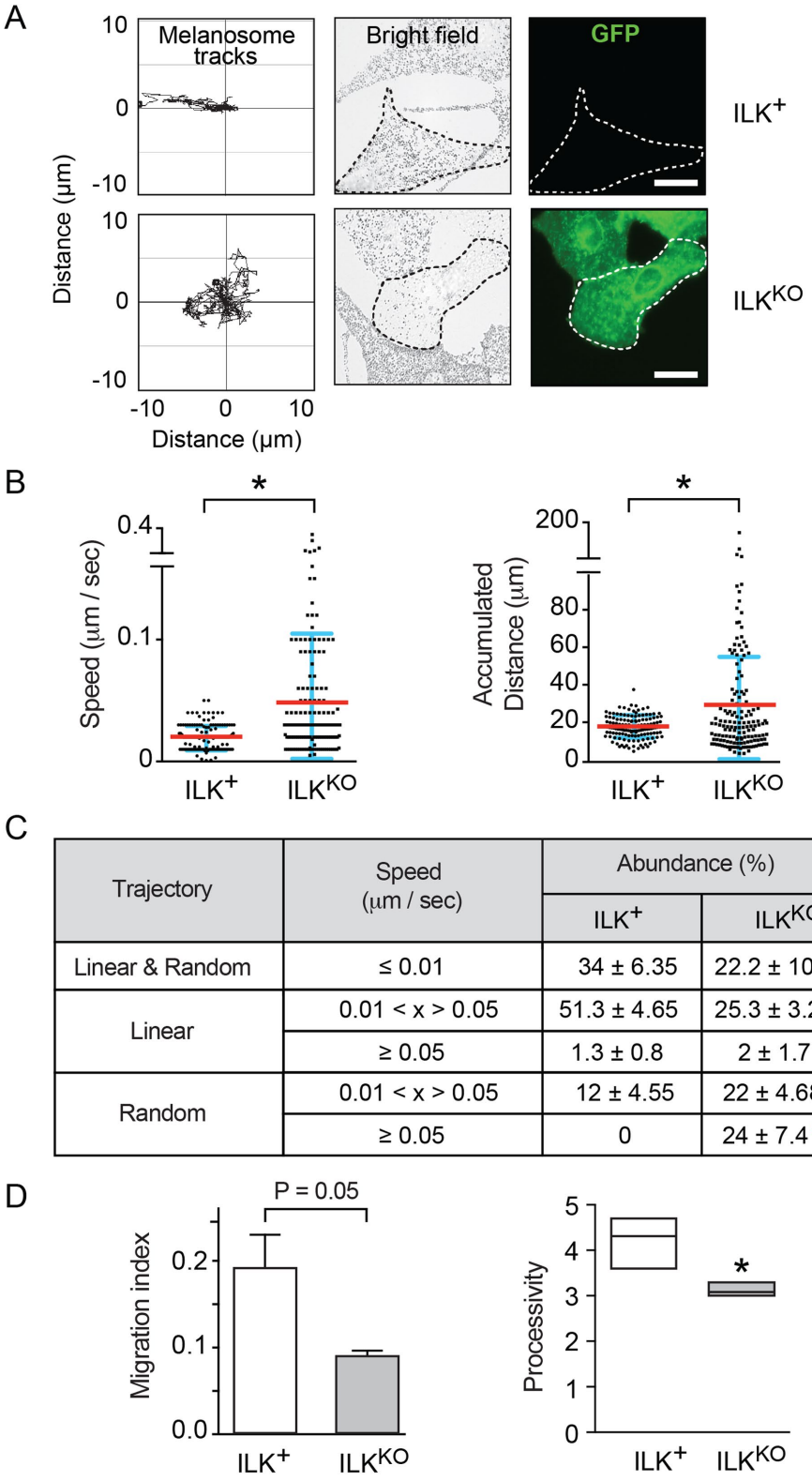

Trajectory	Speed (μm / sec)	Abundance (%)	
		ILK^+	ILK^{KO}
Linear & Random	≤ 0.01	34 ± 6.35	22.2 ± 10.5
Linear	0.01 < x > 0.05	51.3 ± 4.65	25.3 ± 3.29 *
	≥ 0.05	1.3 ± 0.8	2 ± 1.7
Random	0.01 < x > 0.05	12 ± 4.55	22 ± 4.68
	≥ 0.05	0	24 ± 7.4 *

FIGURE 1: Altered melanosome dynamics in ILK^{KO} melanocytes. Epidermal melanocytes were cultured on laminin-332–coated surfaces in the absence or presence of 1 μM 4OHT for 48 h, followed by 72 h in the absence of the drug, to generate ILK^+ or ILK^{KO} cells, respectively. Time-lapse micrographs were recorded during a 10-min interval (6 frames/min) to analyze melanosome movements (150 melanosomes from four independent cell isolates). (A) Representative trajectory plots of melanosomes from the ILK^+ and GFP-expressing ILK^{KO} cells shown in the accompanying micrographs. Bar, 20 μm. (B) Average speed and total distance traveled by individual melanosomes. V_{Avg} and SD values are represented by red and blue lines, respectively. (C) Relative abundance (mean ± SEM) of melanosomes moving with the indicated trajectory and speed. * indicates $p < 0.05$ relative to the corresponding category in ILK^+ cells. (D) The migration index and processivity of melanosomes are shown as the mean ± SEM. For B and D, * represents $p < 0.05$ relative to ILK^+ cells (Student's *t* test).

cells, as well as in AdCre-transduced ILK-deficient melanocytes (Supplemental Figure 2B). Together, our data indicate that ILK is necessary for normal intracellular distribution of both early- and late-stage melanosomes.

Cytoskeletal characteristics and dynein motor activity in ILK^{KO} melanocytes

Filamentous (F)-actin tracks play key roles in capturing melanosomes from microtubules at dendritic tips and mediating transfer of these organelles to adjacent cells (Wu and Hammer, 2014). We next determined whether loss of ILK affected the actin cytoskeleton, using $Ilk^{f/f}$ melanocytes transduced with AdCre. Examination of the F-actin cytoskeleton in nontransduced ILK-expressing melanocytes revealed the presence of cytoplasmic stress fibers and thick bundles of cortical actin running parallel to the plasma membrane and the long axes of dendrites, and into dendritic tips (Supplemental Figure 2C), consistent with previous reports (Wu *et al.*, 1997). In contrast, cytoplasmic F-actin stress fibers were virtually absent in AdCre-transduced, ILK-deficient cells, whereas thin cortical bundles were visible in a large fraction of these melanocytes. In melanocytes that exhibited pseudopodial extensions, disorganized F-actin aggregates were often present at the tips (Supplemental Figure 2C).

In melanocytes, actin and microtubule transport systems work in a coordinated manner to regulate melanosome movements. Microtubule tracks that extend from perinuclear centrosomal regions to the cell periphery allow bidirectional long-range transport of melanosomes. Because microtubule depletion enhances melanosome dispersion (Evans *et al.*, 2014), we investigated whether loss of ILK is associated with perturbations in the microtubule network. In ILK^+ melanocytes, β-tubulin immunoreactivity formed a densely packed network around the nucleus and decorated clearly defined microtubules that extended into dendritic tips (Figure 3A). In these cells, mature melanosomes were arranged alongside those peripheral microtubule tracks (Figure 3B). In contrast, microtubules in

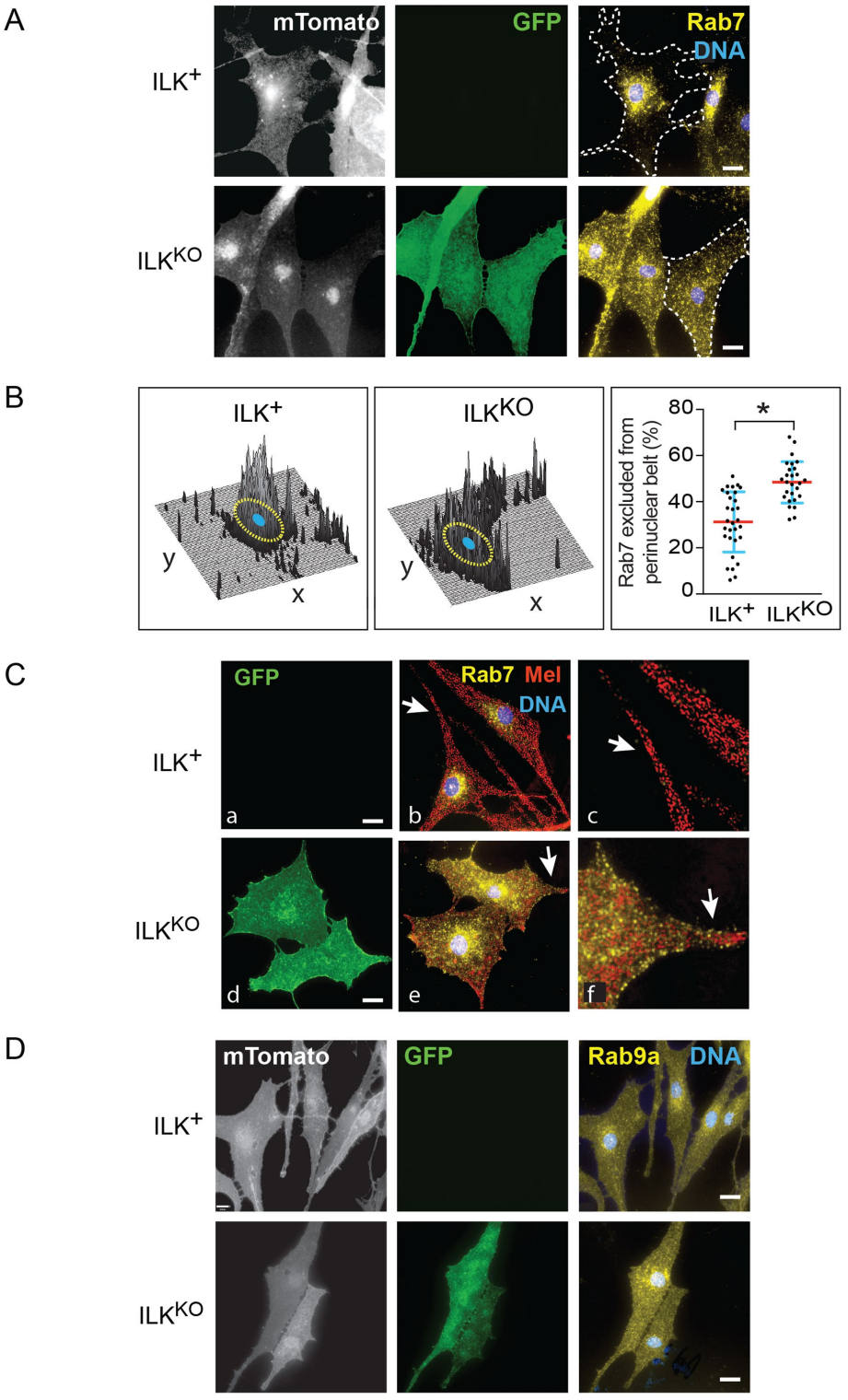

FIGURE 2: Dispersion of Stage I–II melanosomes in ILK^{KO} melanocytes. Epidermal melanocytes were cultured on laminin-332–coated surfaces in the absence or presence of 1 μM 4OHT for 48 h. Following an additional 72-h culture period in the absence of drug, the ILK^{+} or ILK^{KO} cells were processed for immunofluorescence microscopy. (A) Cells were stained with anti-GFP and anti-Rab7 antibodies, DNA was visualized with Hoechst 33342, and mTomato was detected by direct fluorescence. (B) Three-dimensional surface plots representing pixels associated with Rab7 immunoreactivity throughout each of the cells outlined in panel A. The blue ellipse and the dotted lines represent, respectively, the nucleus and the perinuclear belt along the *xy* axes. The accompanying dot plots show the percentage of Rab7-associated pixels that localized outside the perinuclear belt for each of the cells analyzed, with the mean (red lines) and SD (blue lines) values indicated. * represents $p < 0.05$ ($n = 3$, Student's t test). (C) Melanocytes were immunostained with anti-GFP or anti-Rab7 antibodies, whereas melanin-containing stage III–IV melanosomes (Mel; red) were visualized by bright-field microscopy. Arrows indicating cell dendrites in micrographs b and e are shown at higher magnification in micrographs c and f, respectively. (D) Cells were stained with anti-GFP and anti-Rab9a antibodies, DNA was visualized with Hoechst 33342, and mTomato was detected by direct fluorescence. Bars, 10 μm.

ILK^{KO} melanocytes appeared disorganized and less well defined. Further, whereas microtubule tracks longer than 12–20 μm were readily detectable in 40% of normal melanocytes, they were present in only ~10% of ILK^{KO} cells (Figure 3B). As a consequence, a large fraction of mature melanosomes around the cell periphery failed to visibly associate with microtubules (Figure 3B).

The intracellular distribution of melanosomes reflects a balance between centripetal and centrifugal trafficking (Evans *et al.*, 2014). Because centripetal movements involve dynein-mediated transport toward the minus end of microtubules, inhibition of dynein function ultimately causes dispersion of these organelles to the cell periphery (Jordens *et al.*, 2001). Thus, we next explored dynein function in the context of melanosome movements in the absence of ILK. To this end, we used ciliobrevin D for acute inhibition of dynein, avoiding cytotoxicity from prolonged incubation with this drug, and recorded melanosome movements over a 5-min interval. Under these conditions, V_{avg} values of 0.01 ± 0.004 and 0.03 ± 0.003 μm/s were observed, respectively, in vehicle-treated ILK^{+} and ILK^{KO} cells. In the presence of ciliobrevin D, we observed significant >fivefold decreases in melanosome velocity, with V_{avg} values of 0.002–0.003 μm/s, and correspondingly negligible distances migrated, irrespective of whether or not ILK was present (Figure 3C). Collectively, these results indicate that the abnormal melanosome distribution and movements observed in ILK-deficient melanoblasts occur in spite of active transport mediated through dynein motor function.

Decreasing microtubule catastrophe restores melanosome dynamics in ILK^{KO} melanocytes

To determine the effect of stabilizing microtubules on melanosome movements in the absence of ILK, we treated melanocytes with 10 μM paclitaxel for 1 h. Both ILK^{+} and ILK^{KO} cells formed thick microtubule networks that extended to the tips of cell extensions in the presence of this drug (Figure 4A). Significantly, melanin-containing melanosomes in

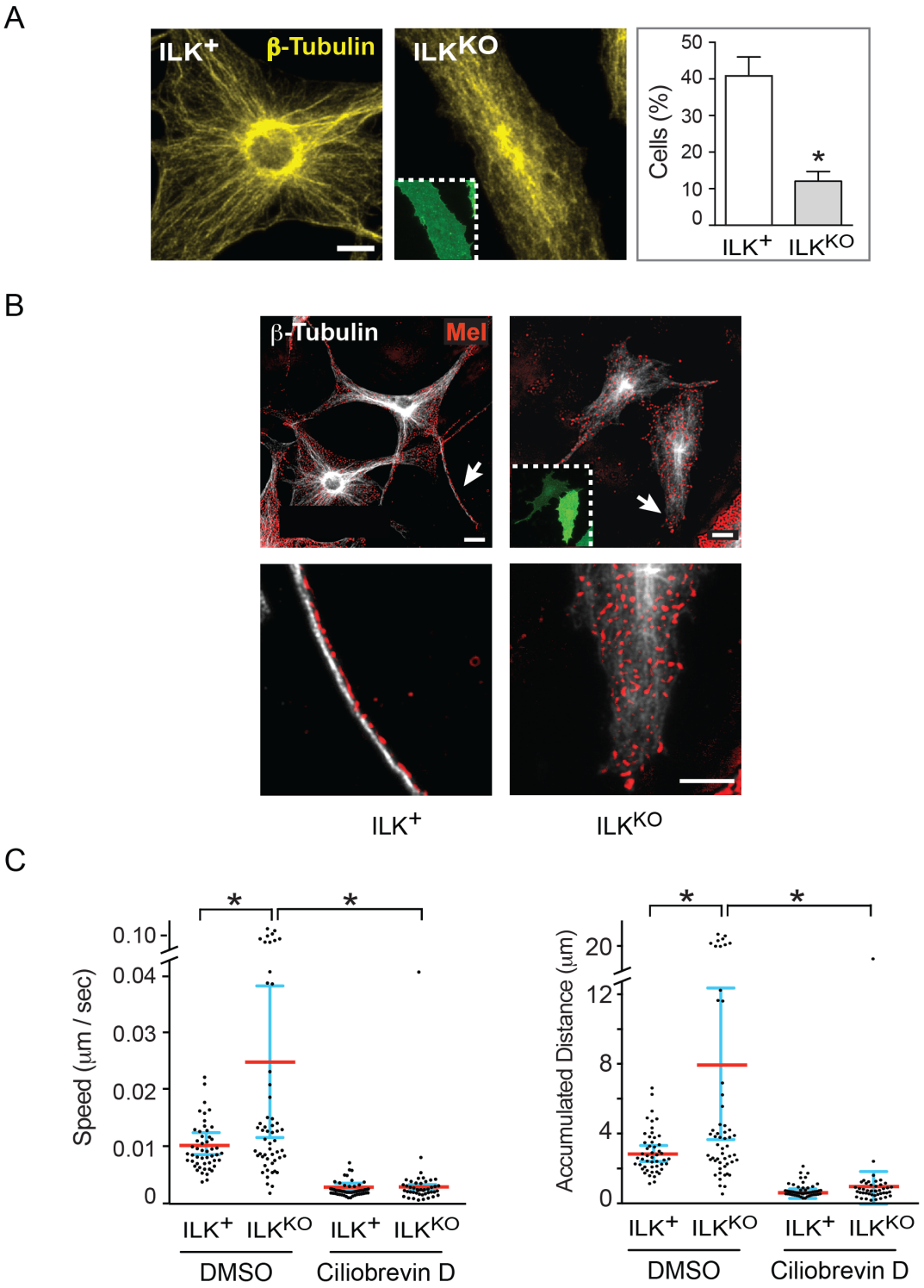

FIGURE 3: Abnormalities in microtubule networks in ILK^{KO} melanocytes. Epidermal melanocytes were cultured on laminin-332–coated surfaces in the absence or presence of 1 μM 4OHT for 48 h, and for 72 h in drug-free medium, to generate ILK^{+} or ILK^{KO} cells. (A) Cells were processed for microscopy with antibodies against β-tubulin or GFP (inset). The accompanying histogram shows the percentage of cells that formed microtubule tracks longer than 2 nuclear diameters (12–20 μm). * represents $p < 0.05$ (Student's t test; $n = 3$). (B) Melanocytes were processed for microscopy as in panel A, and additionally melanin-containing stage III–IV melanosomes (Mel; red) were visualized by bright-field microscopy. Arrows indicate cell dendrites or extensions shown at higher magnification in the accompanying micrographs. Bars, 10 μm. (C) Ciliobrevin D (10 μM) or DMSO (0.1%, final) was added to culture medium 30 min before imaging. Time-lapse images were then obtained during a 10-min interval (6 frames/min) to analyze melanosome movements. The dot plots show the average speed and total distance traveled by individual melanosomes. V_{Avg} and SD values are represented by red and blue lines, respectively. * represents $p < 0.05$ (ANOVA; 50 melanosomes from $n = 3$ independent cell isolates).

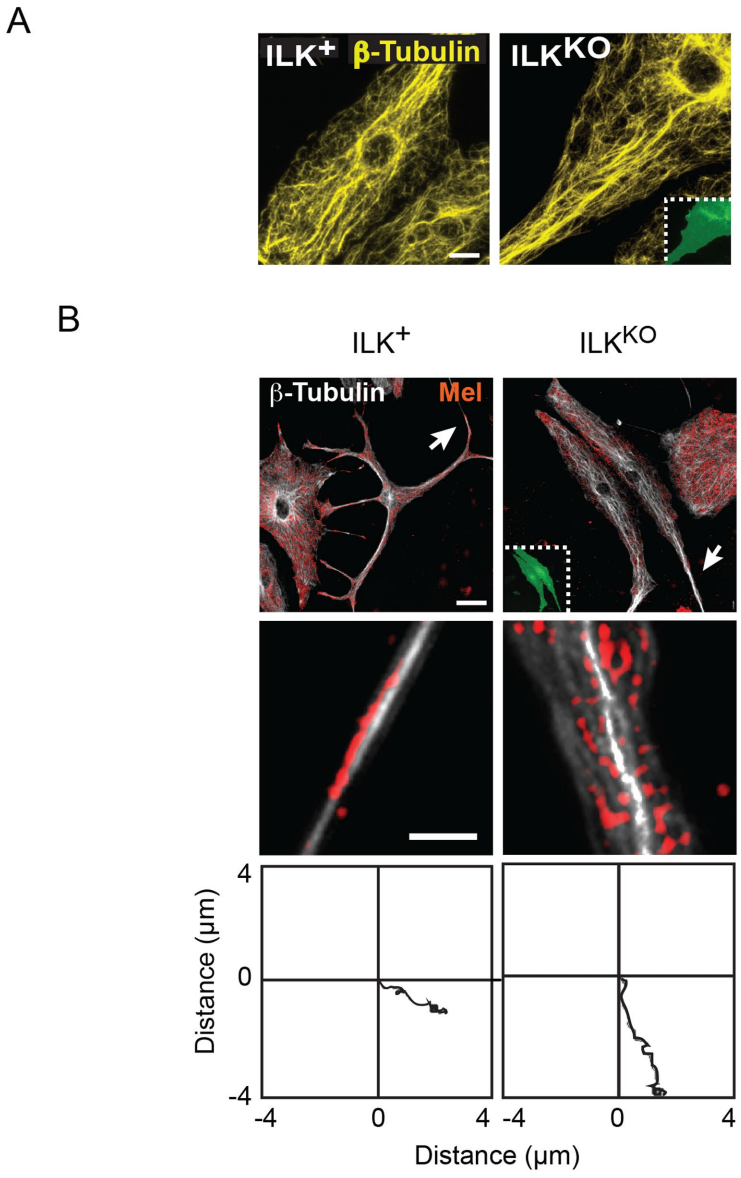

C

Trajectory	Speed (μm / sec)	Abundance (%)			
		ILK^+		ILK^{KO}	
		DMSO	Paclitaxel	DMSO	Paclitaxel
Linear & Random	≤ 0.01	47.6 ± 17.8	35.3 ± 7.3	33.4 ± 8.8	46.0 ± 9.3
Linear	> 0.01	41.4 ± 14.1	51.1 ± 9.3	17.7 ± 5.1	36.8 ± 6.0 *
Random	> 0.01	10.9 ± 4.0	13.6 ± 4.0	48.2 ± 5.4	17.3 ± 4.5 *

FIGURE 4: Effect of microtubule stabilization on melanosome movements in ILK^{KO} melanocytes. Epidermal melanocytes were cultured on laminin-332–coated surfaces in the absence or presence of 1 μM 4OHT for 48 h, and for 72 h in drug-free medium, to generate ILK^+ or ILK^{KO} cells. The cells were then cultured in the presence of 10 μM paclitaxel or control vehicle (0.25% EtOH) for 1 h. (A, B) Representative micrographs of cells probed with antibodies against β-tubulin or GFP (insets). Panel B also shows melanin-containing stage III–IV melanosomes (Mel; red), visualized by bright-field microscopy, as well as representative trajectory plots of melanosomes recorded by live-cell videomicroscopy for 5 min (6 frames/min). Bars, 10 μm. (C) Relative abundance (mean ± SEM) of melanosomes moving with the indicated trajectory and speed. * indicates $p < 0.05$ relative to the corresponding category in ILK^+ cells.

ILK^{KO} cells lined these microtubule tracks efficiently, in a manner that was indistinguishable from those in normal melanocytes (Figure 4B). Analysis of melanosome motility revealed no significant effects of paclitaxel on the proportion of melanosomes docked to the cytoskeleton ($V_{avg} \leq 0.01$ μm/s; ~35%) or with rapid bidirectional movements along microtubule tracks ($V_{avg} > 0.01$ μm/s; ~51%) in ILK^{+} cells (Figure 4C). In ILK^{KO} melanocytes, paclitaxel increased the proportion of melanosomes with rapid bidirectional movements ($V_{avg} > 0.01$ μm/s) to ~37%, while decreasing the fraction of melanosomes with fast random (i.e., oscillatory, nonlinear) movements to ~17%, which was indistinguishable from those in ILK^{+} cells (Figure 4C). Altogether, these studies suggest that microtubule dynamic instability is likely an important factor contributing to the altered melanosome movements observed in the absence of ILK.

Glycogen synthase kinase-3 inhibition and CRMP2 attenuate dendricity deficits in ILK^{KO} melanocytes

Glycogen synthase kinase-3β (GSK-3β) is a well-established regulator of microtubule assembly and dendrite outgrowth in neurons, and inhibition of GSK-3 activity restores microtubule dynamic stability in ILK-deficient epithelial cells (Namekata *et al.*, 2012; Jackson *et al.*, 2015). Analysis of ILK^{KO} cell lysates revealed reduced levels of inactive phosphorylated GSK-3β, consistent with the notion of abnormal GSK-3β regulation in melanocytes in the absence of ILK (Supplemental Figure 3). Given that microtubules are key for melanocyte dendricity, we next determined the consequences of GSK-3 inhibition on dendrite formation in these cells. ILK^{KO} cells seeded on laminin 332 matrix and treated with the GSK-3 inhibitor SB216763 for 24 h displayed a highly dendritic morphology and a well-developed microtubule network that extended to dendritic tips (Figure 5A), without significant changes in total cell surface area or viability, as evidenced by absence of detectable cell nuclei that exhibited fragmented DNA (Supplemental Figure 4).

To further characterize the consequences of GSK-3 inhibition on the ability of melanocytes to form dendrites, we assessed changes in cell circularity (a ratio of cell surface area to perimeter) as a measure indicative of melanocyte dendricity (Robinson *et al.*, 2019). SB216763 treatment of ILK^{+} cells seeded on laminin 332 matrix promoted formation of dendrites, decreasing mean circularity from 0.32 to 0.22 (Figure 5B). In these cultures, 57% and 75% of melanocytes exhibited circularity values ≤0.32 in the absence and presence of SB216763, respectively (Figure 5B). By comparison, the mean circularity value of untreated ILK^{KO} cells was 0.38, significantly higher than that in ILK^{+} melanocytes, in agreement with the recently identified decreased ability of ILK-deficient cells to form dendrites (Crawford *et al.*, 2019). Treatment with SB216763 increased dendricity in ILK^{KO} melanocytes, decreasing mean circularity to 0.26 (Figure 5B). Most notably, in the presence of this GSK-3 inhibitor, the proportion of ILK^{KO} melanocytes with circularity values ≤ 0.32 increased almost twofold to 71%, a fraction indistinguishable from that observed in ILK^{+} cells (Figure 5B). Analogous experiments with melanocytes seeded on culture surfaces without exogenous extracellular matrix substrates showed similar effects of SB21676 treatment (Supplemental Figure 5). Mean circularity values in the absence of exogenous extracellular matrix were somewhat higher than in cells stimulated with laminin 332, in agreement with the ability of the latter to promote melanocyte dendricity (Crawford *et al.*, 2019). Thus, impaired dendrite formation in the absence of ILK can be alleviated significantly through inhibition of GSK-3 activity.

CRMP2 binds to tubulin heterodimers to promote microtubule assembly. In neurons, CRMP2 promotes axon elongation and dendrite formation, and this function is inhibited through phosphorylation of T509 and T514, catalyzed by GSK-3β (Yoshimura *et al.*, 2005; Liz *et al.*, 2014). To determine the role of CRMP2 in the observed GSK-3-associated loss of dendricity in ILK^{KO} cells, we transduced *Ilk$^{f/f}$* melanocytes with AdCre, transfected them 72 h later with vectors encoding CRMP2 proteins, and determined changes in circularity 48 h after transfection. This approach maximized the number of melanocytes that lacked ILK and also expressed exogenous CRMP2. The presence of exogenous wild-type CRMP2 in ILK-expressing cells significantly decreased mean circularity values from 0.29 to 0.15 and increased the proportion of melanocytes with circularity values ≤0.29 from 56% to 80%. In contrast, expression of the phosphomimetic CRMP2 T514D mutant was without effect (Supplemental Figure 6), in agreement with its substantially lower affinity for tubulin (Sumi *et al.*, 2018). The mean circularity value of AdCre-transduced, ILK-deficient melanocytes was 0.37 (Supplemental Figure 6), similar to that observed in 4OHT-treated ILK^{KO} cells. Notably, expression of wild-type CRMP2 in these cells decreased the mean circularity threefold to 0.12, which was indistinguishable from that of ILK-expressing melanocytes. The capacity of CRMP2 T514D to decrease circularity in ILK-deficient melanocytes was substantially weaker (Supplemental Figure 6). Our data are consistent with the notion that GSK-3β and CRMP2 function downstream from ILK to modulate dendricity in primary melanocytes.

Inactivation of *Ilk* disrupts melanin transfer to keratinocytes

Pigment transfer to keratinocytes is a major physiological function of melanocytes. To examine the consequences of abnormal melanosome trafficking in the absence of ILK, we measured changes in melanin uptake by keratinocytes cocultured with melanocytes. Control keratinocyte monocultures exhibited low levels of cytoplasmic dark granules, possibly due to uptake in vivo before isolation, and consistent with the C57BL/6 strain background of donor animals (Figure 6, A and B). We next seeded ILK^{+} or ILK^{KO} melanocytes onto a monolayer of mTomato-expressing keratinocytes isolated from *Tyr::CreER^{T2}; ROSA$^{mT/mG}$; Ilk$^{f/f}$* mice, at a 1:6 ratio, and analyzed by bright-field microscopy the presence of melanin-containing granules in the keratinocytes after 8 h of coculture. Pixels associated with pigmented granules present in keratinocytes cocultured with ILK^{+} melanocytes were 3.5-fold higher than in keratinocyte monocultures during this time. In contrast, no significant increases occurred in keratinocytes in the presence of ILK^{KO} melanocytes during the time frame of these experiments (Figure 6, A and B). This deficiency was not associated with differences in melanin levels, which were comparable in both melanocyte types (Figure 6C).

We next determined the effect of GSK-3 inhibition on pigment transfer to keratinocytes. For these experiments, melanocytes were treated with SB216763 for 24 h, rinsed, trypsinized, and seeded on subconfluent keratinocyte monolayers. Both cell types were then cocultured for 8 h in the absence of drug. In the presence of SB216763, ILK^{KO} melanocytes were able to extend multiple dendrites toward neighboring keratinocytes (Figure 7, A and B). Mean circularity values in vehicle-treated ILK^{+} and ILK^{KO} melanocytes were respectively 0.17 and 0.30 (Figure 7C). In the presence of SB216763, the mean ILK^{KO} cell circularity value decreased to 0.18, indistinguishable from that in ILK^{+} melanocytes. Pixels associated with pigmented granules in keratinocytes cultured with vehicle-treated ILK^{KO} melanocytes were 3.3-fold lower than in those cocultured with ILK^{+} cells (Figure 7D). Inhibition of GSK-3 in ILK^{+} melanocytes reduced pigment transfer to ~65%, relative to vehicle-treated cells. Remarkably, the pigment area in keratinocytes cocultured with

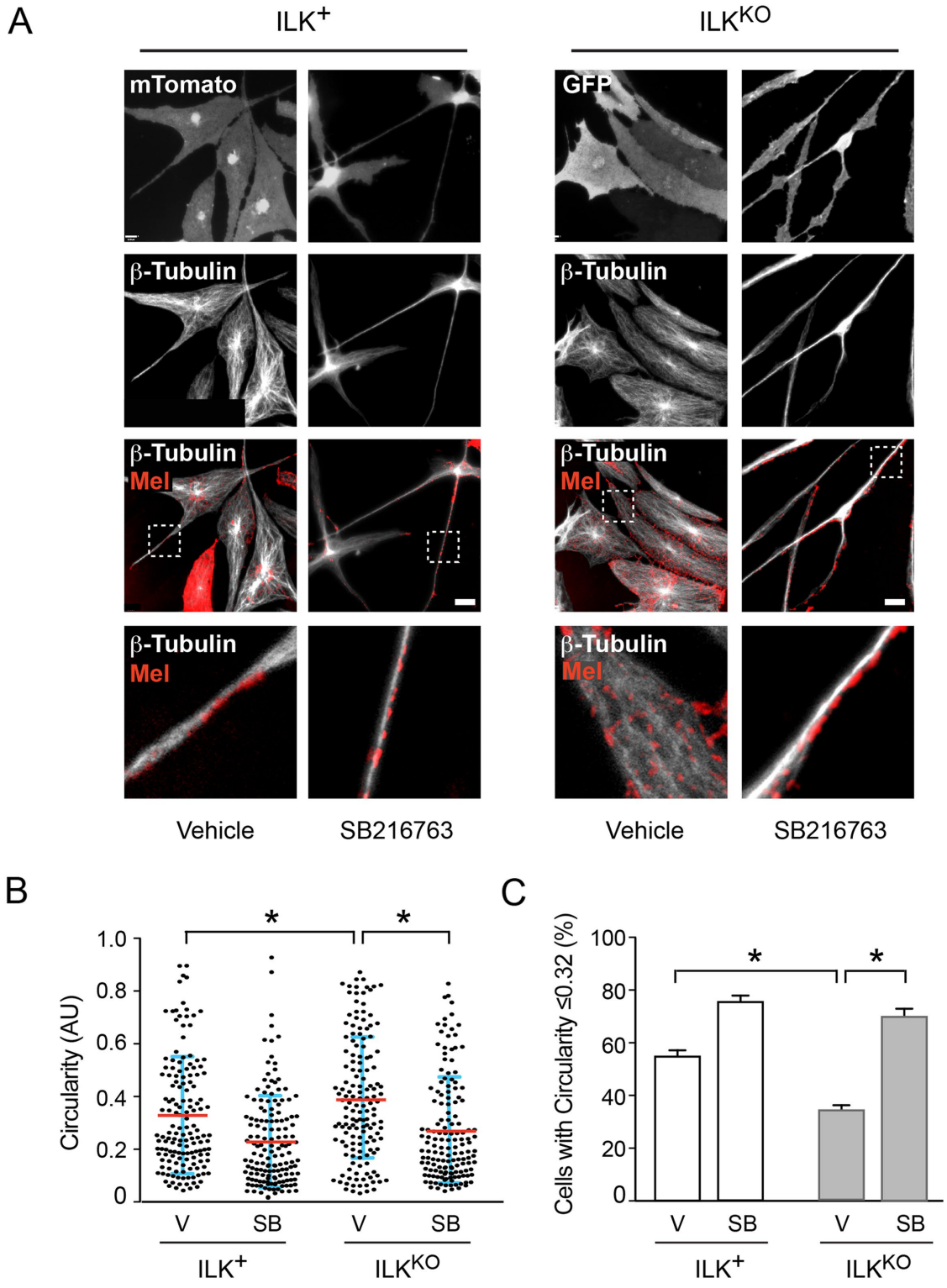

FIGURE 5: Inhibition of GSK-3 restores dendricity in ILK^{KO} melanocytes. Primary melanocytes were cultured on surfaces coated with laminin-332 matrix, in the absence or presence of 1 μM 4OHT for 48 h, and for another 48-h interval in drug-free medium, to generate ILK^{+} or ILK^{KO} cells. The cells were then treated with control DMSO vehicle (V) or 5 μM SB216763 (SB) for 24 h and processed for microscopy. (A) Representative micrographs of melanocytes visualized through direct mTomato fluorescence or processed with antibodies against GFP or β-tubulin, as indicated. Melanin-containing stage III–IV melanosomes (Mel; red) were visualized by bright-field microscopy. Boxed areas are shown at higher magnification in the micrographs directly underneath each treatment column. Bar, 10 μm. (B) Dot plots showing circularity values of individual ILK^{+} and ILK^{KO} melanocytes. The mean and SD are indicated, respectively, by the red and blue bars. * indicates $p < 0.05$ (ANOVA; 90 melanocytes scored per group in three experiments using independent cell isolates). (C) Percentage of melanocytes with circularity values ≤ 0.32, which corresponds to the average observed in vehicle-treated ILK^{+} melanocytes. The data are shown as the mean + SEM, and * indicates $p < 0.05$ (ANOVA).

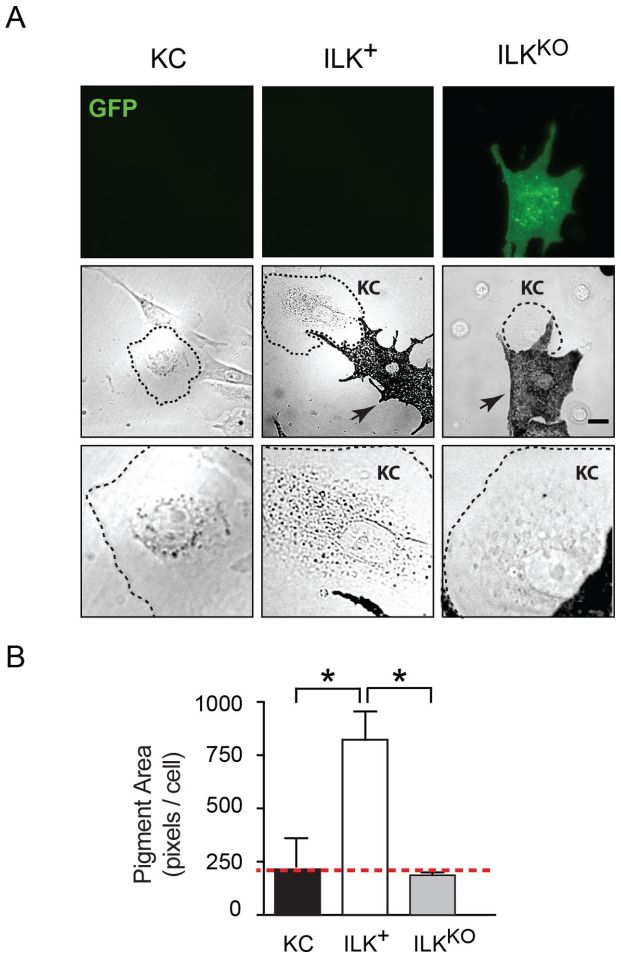

FIGURE 6: Impaired melanin transfer from ILK^{KO} melanocytes. Epidermal melanocytes were cultured in the absence or presence of 1 μM 4OHT for 48 h, and for 72 h in drug-free medium, to generate ILK^{+} or ILK^{KO} cells. The cells were trypsinized, seeded onto a subconfluent monolayer of primary mouse keratinocytes, cocultured for 8 h, and then processed for microscopy. (A) Representative micrographs of keratinocyte monocultures (KC) or keratinocytes cocultured with ILK^{+} or ILK^{KO} melanocytes, stained with anti-GFP antibodies. In the corresponding bright-field images, dashed lines outline keratinocytes (KC), and arrows indicate melanocytes. Accompanying higher magnification images are also shown. Bar, 20 μm. (B) Quantification of the area occupied by pigmented granules in keratinocytes cultured in the absence (KC) or presence of ILK^{+} or ILK^{KO} melanocytes. The results are expressed as the mean + SEM (100 keratinocytes scored from four independent experiments). * indicates $p < 0.05$ (ANOVA).

SB216763-treated ILK^{KO} melanocytes increased almost twofold, to levels indistinguishable from those in cocultures containing ILK^{+} melanocytes (Figure 7D). Our observations are consistent with the notion that GSK-3 is involved in melanin transfer and that inhibition of GSK-3 activity in ILK^{KO} melanocytes partially restores their ability to form dendrites and transfer melanin to neighboring keratinocytes.

DISCUSSION

In the present studies we developed a reporter cell model for inducible inactivation of the *Ilk* gene, which allowed us to investigate how scaffold modulators of cytoskeletal dynamics contribute to melanosome trafficking in primary mammalian melanocytes. With the combined use of time-lapse microscopy and melanosome tracking, we also developed an algorithm to assess processivity of melanosome movements in an unbiased and quantitative manner. This method has the potential to analyze cytoplasmic organelle trafficking associated with microtubule tracks. The novel findings of our studies are threefold.

First, we discovered that ILK is required for perinuclear retention of early-stage melanosomes, without affecting melanin biosynthesis per se. Stage I–II melanosomes cluster around the perinuclear area and remain closely associated with the microtubule organizing center, allowing delivery of structural and enzymatic components. Early melanosomes are anchored on microtubules around the nucleus through the action of tripartite complexes composed of Rab7, Rab-interacting lysosomal protein, and the microtubule minus end–directed motor protein dynein (Watabe *et al.*, 2008). When dynein activity is abrogated, early melanosomes move away from the nucleus and toward the cell periphery (Jordens *et al.*, 2006). Although we did not directly measure dynein motor activity in ILK^{KO} cells, the loss of melanosome motility in ciliobrevin D–treated cells suggests that dynein is functional in the absence of ILK. In melanophores, aggregation of melanosomes around perinuclear regions requires their capture to microtubule plus ends, thus initiating and/or enhancing minus end–directed transport. Central for this process are microtubule plus end tracking proteins (+TIPs), such as Clip-170, together with maintenance of normal microtubule dynamics (Lomakin *et al.*, 2009). ILK is a scaffold protein involved in microtubule organization, and its absence leads to increased frequency of microtubule catastrophe at the plus ends and dynamic instability (Wickstrom *et al.*, 2010; Jackson *et al.*, 2015). We propose that enhanced microtubule depolymerization may occur in ILK^{KO} melanocytes, potentially leading to the release of Stage I–II melanosomes from microtubule tracks, eventually facilitating their dispersion throughout the cytoplasm. Whether the absence of ILK results in additional alterations in the processes that regulate subcellular distribution of early melanosomes remains an important area to be explored.

Second, we observed that normal linear movements and association of Stage III–IV melanosomes with microtubule tracks requires ILK. In the absence of ILK, microtubules do not appear to completely extend to the cell periphery, and melanosomes exhibit deficits in directional movements, showing instead random trajectories and greater speed. This pattern may occur as a result of altered melanosome tethering to microtubules and/or or melanosome switching of microtubule tracks as a consequence of increased depolymerization. Consistent with this proposal, paclitaxel-induced microtubule stabilization and suppression of catastrophe frequency (Risinger *et al.*, 2014) restored melanosome directional movements and processivity. In the steady state, and in the absence of external signals, melanosomes are shuttled back and forth, with little net displacement due to the relative activity of the various motor proteins associated with these organelles (Barlan and Gelfand, 2017). Maintenance of a uniform melanosome distribution throughout the cell requires coordinate contributions from the F-actin and microtubule cytoskeletons. Melanosomes that reach dendritic tips moving along microtubules can be transferred to peripheral F-actin fibers, where they are tethered through the action of tripartite capture complexes containing Rab27a, melanophilin, and myosin Va (Robinson *et al.*, 2019). Disruption of these complexes causes a loss of melanosomes in dendrites and impaired pigment transfer to keratinocytes (Barlan and Gelfand, 2017). The decreased ability of microtubules to reach dendritic tips may conceivably be associated with reduced transfer of melanosomes to actin fibers in ILK^{KO} melanocytes. Our studies place ILK as an important determinant of organelle trafficking, through its role in stabilization of microtubules. Similarly, ILK is

necessary for plasma membrane targeting of recycling endosomes containing E-cadherin and, in its absence, adherens junction formation is impaired in epidermal keratinocytes (Ho *et al.*, 2016). ILK also contributes to trafficking of caveolae to the plasma membrane in keratinocytes and endothelial cells (Wickstrom *et al.*, 2010; Malan *et al.*, 2013). Thus, the contribution of ILK to cytoskeletal integrity is essential for trafficking and delivery of multiple organelles to appropriate subcellular locations.

Third, we have identified GSK-3 as a modulator of melanocyte dendricity. Melanocytes and neurons share common embryonic origins, as well as signaling pathways that allow them to home to the appropriate target tissues, sprout dendrites, and form connections with neighboring cells (Yaar and Park, 2012). In neurons, decreased GSK-3β activity is necessary for microtubule-dependent neurite and axonal growth and regeneration (Ma *et al.*, 2007; Namekata *et al.*, 2012; Liz *et al.*, 2014). In these cells, Fyn kinase/Dock3/Rac1 complexes are activated by receptor tyrosine kinase stimulation, resulting in membrane recruitment, phosphorylation, and inhibition of GSK-3β (Namekata *et al.*, 2012). In ILK-deficient epidermal keratinocytes, reduced levels of phosphorylated GSK-3β are also found, but they can be restored by exogenous expression of constitutively active Rac1 proteins (Jackson *et al.*, 2015). In these cells, ILK functions as an adaptor protein that brings together ELMO2/Rho-G-containing complexes, which contribute to Rac1 activation in response to epidermal growth factor receptor stimulation (Ho and Dagnino, 2012). Thus, in melanocytes, ILK may regulate microtubules functioning as a scaffold that contributes to interactions between Rho family GTPases and other proteins that regulate GSK-3. According to this model, ILK may be key for coordinated Rac1-dependent GSK-3β inhibition and CRMP2-mediated extension of plus ends, similarly to its role in epidermal keratinocytes (Jackson *et al.*, 2015). GSK-3 modulates the activity of various microtubule-associated proteins, including CRMP2, CRMP4, MAP1B,, and CLASP2 (Liu *et al.*, 2012). Loss of ILK in melanocytes leads to deregulation of GSK-3 activity and loss of dendricity. Our studies suggest a role for GSK-3 and CRMP2 in dendrite formation in these cells, although further studies are necessary to address the potential role of other GSK-3 substrates in this process. Finally, our studies have also shown the contribution of GSK-3 activity to melanin transfer from melanocytes to keratinocytes, in addition to its established roles in modulating MITF expression and melanin synthesis (Cao *et al.*, 2017), thus uncovering a novel important role for this kinase in fundamental melanocyte functions in the epidermis.

MATERIALS AND METHODS

Mouse strains

All animal experiments were approved by the University of Western Ontario Animal Care Committee (Protocol No. 2018-169), according to regulations and guidelines of the Canadian Council on Animal Care. Mouse strains were genotyped as described (Crawford *et al.*, 2019). *Tyr::CreER^{T2}; Ilk$^{f/f}$* mice were generated by breeding to homozygosity *B6.Cg-Tg(Tyr-cre/ERT2)13Bos/J Tyr::CreER^{T2}* mice (purchased from the Jackson Laboratory, Stock 02328, Bar Harbor, ME) (Bosenberg *et al.*, 2006) with *Ilk^{tm1Star}* mice, in which the *Ilk* gene is flanked by loxP sites (Terpstra *et al.*, 2003). The *Tyr::CreER^{T2}; ROSA$^{mT/mG}$; Ilk$^{f/f}$* reporter mouse strain, which is homozygous for the *Tyr::CreER^{T2}*, *ROSA$^{mT/mG}$*, and *Ilk^{tm1Star}* alleles has been previously described (Crawford *et al.*, 2019).

Reagents and antibodies

Melanocyte basal medium (C-24210) was purchased from PromoCell (Sickingenstr, Heidelberg, Germany). Melanocyte growth supplements (CC-4435) and endothelin-3 (CC-4510) were from Lonza (Walkersville, MD). (Z)-4-hydroxytamoxifen (4OHT; ab141943) was purchased from Abcam (Cambridge, UK). Trypsin (0.025%)/EDTA (0.01%) solution (R-001-100) and trypsin neutralizer solution (R-002-100) were from Life Technologies/Thermo Fisher (Carlsbad, CA). Ciliobrevin D (250401), paclitaxel (33069-62-4), X-tremeGene 9, and all other chemicals were from Millipore Sigma (Burlington, MA). The GSK-3β inhibitor SB216763 (1616) was from Tocris Biosciences (Bristol, UK). Immu-mount mounting medium (9990402) was from Fisher Scientific (Ottawa, ON, Canada). Antibodies and their sources were as follows: Chicken antibody against green fluorescent protein (GFP; Cat. No. 13970), from Abcam (Cambridge, UK); mouse anti-Rab7 (sc-376362), from Santa Cruz Biotechnology (Dallas, TX); the E7 hybridoma that produces anti–β-tubulin, developed by M. Klimkowsky, was from the Developmental Studies Hybridoma Bank, created by the National Institute of Child Health and Human Development of the National Institutes of Health (NIH), and maintained at the University of Iowa, Department of Biology (Iowa City, IA). Mouse anti- glyceraldehyde 3-phosphodehydrogenase (GAPDH; ADI-CSA-335-E) was purchased from Enzo Life Sciences (Brockville, ON, Canada). Rabbit anti–phospho-GSK-3β (Ser-9, 9336), mouse anti–GSK-3β (9832), and rabbit monoclonal anti-Rab9a (5118S) antibodies were from Cell Signaling Technology (Danvers, MA). Alexa Fluor-conjugated goat anti-mouse and goat anti-chicken IgG were from Molecular Probes/Invitrogen (Eugene, OR).

Adenoviral and plasmid vectors

The recombinant adenovirus encoding GFP-tagged Cre recombinase (AdCre, Catalogue No. 1700) was from Vector Biolabs (Philadelphia, PA). The plasmid encoding Dsred-tagged melanophilin (pDsred monomer C1–MLPH) was a gift from William Gahl (Medical Genetics Branch, National Human Genome Research Institute, NIH; Addgene plasmid #89236; http://n2t.net/addgene:89236; RRID:Addgene 89236), and was verified by dideoxy sequencing. The vectors encoding FLAG-tagged wild-type, T514A and T514D CRMP2 were generous gifts from M.M. Sousa (Instituto de Biologia Molecular e Celular, Porto, Portugal) and have been described by Liz *et al.* (2014).

Cell isolation, culture, and drug treatments

Mouse epidermal melanocytes were isolated and cultured as previously described (Crawford *et al.*, 2017; Dagnino and Crawford, 2019). All experiments were conducted with passage 2-3 cultures, which were composed of ≥95% exponentially proliferating (nonsenescent) melanocytes (Crawford *et al.*, 2017). Where indicated, melanocytes were plated on culture surfaces coated with laminin-332 matrix present in conditioned medium from 804G rat bladder squamous carcinoma cells (Dagnino and Crawford, 2019). To induce Cre-mediated recombination, melanocytes were cultured in medium containing 1 µM 4OHT or 0.25% ethanol (control vehicle) for 48 h, followed by a PBS rinse and further culture in melanocyte growth medium for 72 h before experiments were conducted, unless otherwise stated in individual experiments. ILK-deficient melanocytes were identified through GFP fluorescence. Where indicated, melanocytes were incubated at 37°C with 10 µM paclitaxel for 1 h, or with 10 µM Ciliobrevin D for 30 min before time-lapse live cell imaging. For experiments using GSK3 inhibitors, melanocytes were cultured in medium with growth supplements and incubated in the presence of 5 µM SB216763 or 0.013% dimethylsulfoxide (DMSO) control vehicle for 24 h. The cells were then processed for microscopy analysis or trypsinized and used in melanocyte/keratinocyte coculture experiments.

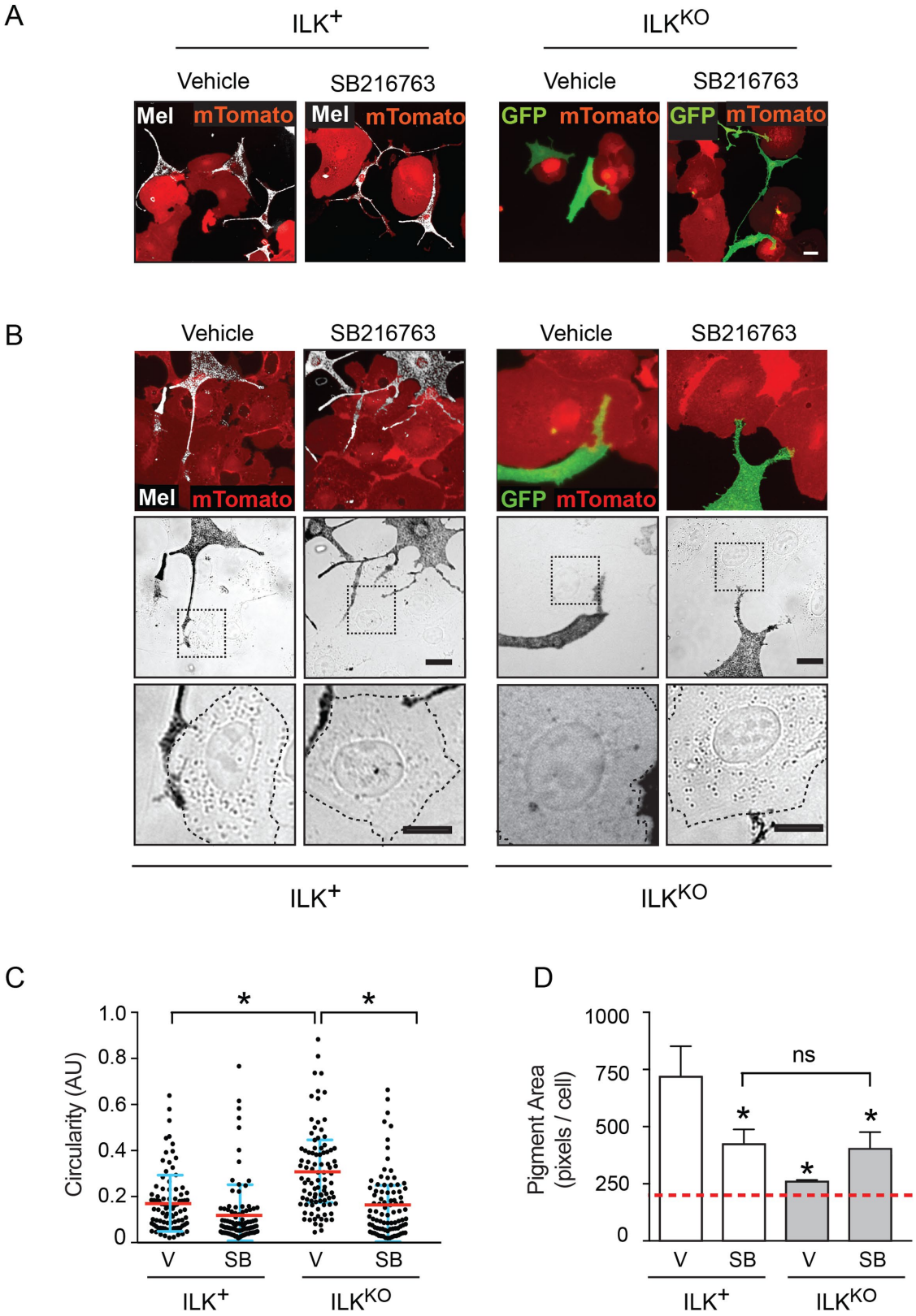

FIGURE 7: Effects of GSK-3 inhibition on melanin transfer. Epidermal melanocytes were sequentially treated with 1 μM 4-OHT and either DMSO vehicle (V) or 5 μM SB216763 (SB), as in Figure 5. The cells were trypsinized, seeded onto a subconfluent monolayer of primary mouse keratinocytes at a 1:6 ratio, cocultured in the absence of drugs for 8 h, and then processed for microscopy. (A, B) Representative bright-field and fluorescence microscopy images showing keratinocytes identified through mTomato direct fluorescence, ILK^{+} melanocytes indicated with arrows, and also identified by the presence of Stage III–IV melanin-containing melanosomes (Mel; white). ILK^{KO} melanocytes are identified by GFP immunoreactivity. Accompanying higher magnification images are also shown. Bars, 20 μm. (C) Dot

Primary epidermal keratinocytes were isolated from 4-d-old mice, and cultured in Ca^{2+}-free Eagle's MEM (06-174G, Lonza, Rockland, ME) supplemented with growth additives and 8% fetal bovine serum pretreated with Chelex-100 ion-exchange resin (1422832, Bio-Rad Laboratories, Mississauga, ON, Canada), as previously described (Vespa *et al*., 2005).

Transfection and viral transduction of melanocytes

For adenoviral transduction, cells were cultured for 4 h in the presence of AdCre virus diluted in melanocyte growth medium, at a multiplicity of infection (MOI) of 120. Following a PBS rinse, the cells were cultured in normal growth medium for 5 d. Under these conditions, transduction efficiency was ≥95%, with no significant cytotoxicity. Sequential transduction and transfection of melanocytes were conducted as described by Dagnino and Crawford (2019), with minor modifications. Cells were seeded in 24-well culture dishes at a density of 25,000 cells/cm^2 and transduced with AdCre as above, but 72 h after transduction, the cells in each well were transfected with 1.5 µg plasmid DNA and 4.5 µl X-tremeGene 9. Melanocytes were processed for microscopy 48 h after the initial addition of plasmid DNA.

Fluorescence microscopy and image analysis

For epifluorescence and indirect immunofluorescence microscopy analyses, melanocytes were fixed in freshly diluted 4% paraformaldehyde and processed as described by Sayedyahossein *et al*. (2015). Fluorescence, bright-field, and phase-contrast micrographs were obtained with a Leica DMIRBE fluorescence microscope equipped with an ORCA-ER digital camera (Hamamatsu Photonics), using Volocity 6.1.1 software (Improvision).

To measure cell circularity, the area and perimeter of each cell imaged were determined from cell outlines generated using the freehand tool of FIJI/ImageJ software version 1.50i (Fiji, National Institutes of Health; Schindelin *et al*., 2012; Rueden *et al*., 2017). Circularity values for individual cells were calculated with the formula $4\pi A/P^2$, where A = cell area and P = cell perimeter (Robinson *et al*., 2019).

To analyze clustering and distribution of Rab7-positive vesicles, which mainly represent stage I-II melanosomes (Jordens *et al*., 2006), we first examined images of Rab7 immunoreactivity in a random population of normal melanocytes, which showed predominantly perinuclear Rab7-positive melanosome clusters, and visualized nuclear DNA with Hoechst 33342 staining, using a high-resolution Plan-Apochromat 63x/1.32 Oil PH3 objective (Leica). We determined that a majority of Rab7-positive melanosomes were distributed around the nucleus within an elliptical area termed the "perinuclear belt," defined by minor and major radii equal to *2r* (where *r* represents the minor radius of the nucleus) and *2R* (where *R* represents the major radius of the nucleus), respectively. For each melanocyte imaged, pixels corresponding to Rab7-associated immunoreactivity found within and outside the perinuclear belt were quantified using ImageJ.

Analysis of melanosome movements

Cells were seeded onto 35-mm µ-Dishes (81156; ibidi GMBH, Madison, WI) precoated with laminin 332-substrate at a density of 30,000 cells/dish, cultured for 24 h, and then treated with 4OHT as described above. For live-cell imaging, melanocytes on a heated/CO_2 perfused microscope stage were maintained at 37°C in a humidified 5% CO_2 atmosphere. Bright-field and fluorescence time-lapse micrographs were obtained at 5- or 10-min intervals at a rate of 6 frames/min with a Nikon Eclipse Ti inverted microscope and a Plan-Apochromat VC 100×/1.4 Oil DIC N2 objective at the Functional Proteomics Facility, Department of Biochemistry, University of Western Ontario. Micrographs were acquired with NIC-Elements Imaging Software version 4.20 (Nikon Instruments, Melville, NY). The resulting time-lapse images were exported as tagged image file formatted image stacks. Melanosomes were manually tracked using the Manual Tracking plugin for ImageJ software, version 1.50i (Fiji, NH). The speed and the accumulated and Euclidian distance for each melanosome were calculated using the ImageJ Chemotaxis & Migration Tool (version 1.48; ibidi GMBH, Madison, WI).

Single-particle melanosome trajectories were quantified using mean-squared displacement (MSD) and processivity analysis, implemented using our previously published algorithms in a custom-written Matlab script (Goiko *et al*., 2016, 2018). Briefly, the movements of individual melanosomes were manually tracked with the Manual Tracking plugin for ImageJ software, as described above, and the resulting files were imported into Matlab. Directionality of melanosome movement was quantified by three different measures. First, the MSD for individual melanosomes was calculated for lag-times (τ) of <time of 1 video frame> to the total length of the melanosome track, defined as follows:

$$\overline{r^2\tau} = \left\langle \left(x(t'+\tau)-x(t')\right)^2 + \left(y(t'+\tau)-y(t')\right)^2 \right\rangle$$

Melanosome movement was then classified based on the fitting of MSD and τ to a single-power model, with powers <1 indicating random motion, and powers >1 indicating linear motion (Goiko *et al*., 2016). Processivity was calculated by scoring the average number of frames where the melanosome moved in the same direction ± 45°. Finally, the migration index was calculated as the ratio of the displacement of the melanosome over the duration of the track to the total distance moved by the melanosome over the duration of the track, using the following equation:

$$\text{Migration index} = \frac{\left((x_n-x_0)^2+(y_n-y_0)^2\right)^{1/2}}{\sum_{1\le n\le m}^{m}\left((x_n-x_{n-1})^2+(y_n-y_{n-1})^2\right)^{1/2}}$$

For each experiment, ≥50 melanosomes from ≥5 cells were tracked.

Melanin quantification

Melanocytes were lysed in an aqueous solution containing 1 M NaOH and 10% DMSO, as described by Crawford *et al*. (2017). The melanin concentration in the lysates was determined from absorbance measurements at 420 nm; the values obtained were interpolated with those from a synthetic melanin standard curve. The results were normalized to cell number.

plots showing circularity values of individual ILK^+ and ILK^{KO} melanocytes in the cocultures. The mean and SD are indicated, respectively, by the red and the blue bars. * indicates $p < 0.05$ (ANOVA; 90 melanocytes scored per group in three experiments using independent cell isolates). (D) Quantification of the area occupied by pigmented granules in keratinocytes cultured in the presence of ILK^+ or ILK^{KO} melanocytes. The results are expressed as the mean + SEM (75 keratinocytes in each group, scored from three experiments with independent cell isolates). The dashed line represents the mean pigment area in keratinocyte monocultures. * indicates $p < 0.05$ relative to pigment area in keratinocytes cocultured with DMSO-treated ILK^+ melanocytes; ns, not significant (ANOVA).

Analysis of melanin transfer to keratinocytes

Primary epidermal keratinocytes were seeded in 24-well μ-plates (82046; ibidi GMBH, Madison, WI) at a density of 50,000 cells/cm^2 and cultured for 3–4 d. After removal of the culture medium, keratinocytes were rinsed with PBS. Trypsinized melanocytes suspended in melanocyte medium containing growth supplements (10,000–20,000 cells) were seeded onto the keratinocyte monolayers. Under these conditions, melanocyte:keratinocyte ratios were typically 1:6. After 8 h of coculture at 37°C, the cells were fixed and processed for microscopy. To evaluate melanosome uptake, the surface area occupied by pigment granules in keratinocytes was determined from bright-field images, similarly to previously described protocols (Tarafder *et al*., 2014), and expressed in pixels/cell, using the Analyze Particle function of ImageJ.

Statistical analyses

Data were analyzed using Student's *t* test or one- or two-way analysis of variance (ANOVA) with post hoc Tukey correction as appropriate, using Graphpad Prism version 6.0c software. Significance was set at $p < 0.05$. All experiments were conducted in duplicate or triplicate samples at least three times, using independent cell isolates.

ACKNOWLEDGMENTS

We thank S. Sayedyahossein for comments on the manuscript. M.C. was supported by an Internal Grant from the Lawson Health Research Institute (Grant F0588) awarded to M.C. and L.D., by a "Quality of Life Trainee Support" grant from the Children's Health Research Institute funded by the Children's Health Foundation, awarded to L.D., and by an Ontario Graduate Scholarship. N.L. was the recipient of an Undergraduate Student Research Award from the Natural Sciences and Engineering Research Council of Canada (NSERC). This work was funded by an NSERC Discovery Grant (RGPIN-2017-04765) and by a Medical and Health Sciences Research Board Accelerator Research Grant from Western University awarded to L.D.

REFERENCES

Barlan K, Gelfand VI (2017). Microtubule-based transport and the distribution, tethering, and organization of organelles. Cold Spring Harb Perspect Biol 9, a025817.

Bosenberg M, Muthusamy V, Curley DP, Wang Z, Hobbs C, Nelson B, Nogueira C, Horner JW II, DePinho R, Chin L (2006). Characterization of melanocyte-specific inducible Cre recombinase transgenic mice. Genesis 44, 262–267.

Bruder JM, Pfeiffer ZA, Ciriello JM, Horrigan DM, Wicks NL, Flaherty B, Oancea E (2012). Melanosomal dynamics assessed with a live-cell fluorescent melanosomal marker. PLoS One 7, e43465.

Cao J, Tyburczy ME, Moss J, Darling TN, Widlund HR, Kwiatkowski DJ (2017). Tuberous sclerosis complex inactivation disrupts melanogenesis via mTORC1 activation. J Clin Invest 127, 349–364.

Correia MS, Moreiras H, Pereira FJC, Neto MV, Festas TC, Tarafder AK, Ramalho JS, Seabra MC, Barral DC (2018). Melanin transferred to keratinocytes resides in nondegradative endocytic compartments. J Invest Dermatol 138, 637–646.

Crawford M, Leclerc V, Barr K, Dagnino L (2019). Essential role for integrin-linked kinase in melanoblast colonization of the skin. J Invest Dermatol 140, 425–434.e10.

Crawford M, Leclerc V, Dagnino L (2017). A reporter mouse model for in vivo tracing and in vitro molecular studies of melanocytic lineage cells and their diseases. Biol Open 6, 1219–1228.

Dagnino L, Crawford M (2019). Isolation, culture, and motility measurements of epidermal melanocytes from GFP-expressing reporter mice. Methods Mol Biol 1879, 243–256.

Evans RD, Robinson C, Briggs DA, Tooth DJ, Ramalho JS, Cantero M, Montoliu L, Patel S, Sviderskaya EV, Hume AN (2014). Myosin-Va and dynamic actin oppose microtubules to drive long-range organelle transport. Curr Biol 24, 1743–1750.

Goiko M, de Bruyn JR, Heit B (2016). Short-lived cages restrict protein diffusion in the plasma membrane. Sci Rep 6, 34987.

Goiko M, de Bruyn JR, Heit B (2018). Membrane diffusion occurs by continuous-time random walk sustained by vesicular trafficking. Biophys J 114, 2887–2899.

Gomez PF, Luo D, Hirosaki K, Shinoda K, Yamashita T, Suzuki J, Otsu K, Ishikawa K, Jimbow K (2001). Identification of rab7 as a melanosome-associated protein involved in the intracellular transport of tyrosinase-related protein 1. J Invest Dermatol 117, 81–90.

Hida T, Sohma H, Kokai Y, Kawakami A, Hirosaki K, Okura M, Tosa N, Yamashita T, Jimbow K (2011). Rab7 is a critical mediator in vesicular transport of tyrosinase-related protein 1 in melanocytes. J Dermatol 38, 432–441.

Ho E, Dagnino L (2012). Epidermal growth factor induction of front-rear polarity and migration in keratinocytes is mediated by integrin-linked kinase and ELMO2. Mol Biol Cell 23, 492–502.

Ho E, Ivanova IA, Dagnino L (2016). Integrin-linked kinase and ELMO2 modulate recycling endosomes in keratinocytes. Biochim Biophys Acta 1863, 2892–2904.

Jackson BC, Ivanova IA, Dagnino L (2015). An ELMO2-RhoG-ILK network modulates microtubule dynamics. Mol Biol Cell 26, 2712–2725.

Jordens I, Fernandez-Borja M, Marsman M, Dusseljee S, Janssen L, Calafat J, Janssen H, Wubbolts R, Neefjes J (2001). The Rab7 effector protein RILP controls lysosomal transport by inducing the recruitment of dynein-dynactin motors. Curr Biol 11, 1680–1685.

Jordens I, Westbroek W, Marsman M, Rocha N, Mommaas M, Huizing M, Lambert J, Naeyaert JM, Neefjes J (2006). Rab7 and Rab27a control two motor protein activities involved in melanosomal transport. Pigment Cell Res 19, 412–423.

Liu CM, Hur EM, Zhou FQ (2012). Coordinating gene expression and axon assembly to control axon growth: potential role of GSK3 signaling. Front Mol Neurosci 5, 3.

Liz MA, Mar FM, Santos TE, Pimentel HI, Marques AM, Morgado MM, Vieira S, Sousa VF, Pemble H, Wittmann T, *et al.* (2014). Neuronal deletion of GSK3beta increases microtubule speed in the growth cone and enhances axon regeneration via CRMP-2 and independently of MAP1B and CLASP2. BMC Biol 12, 47.

Lomakin AJ, Semenova I, Zaliapin I, Kraikivski P, Nadezhdina E, Slepchenko BM, Akhmanova A, Rodionov V (2009). CLIP-170-dependent capture of membrane organelles by microtubules initiates minus-end directed transport. Dev Cell 17, 323–333.

Ma C, Wang J, Gao Y, Gao TW, Chen G, Bower KA, Odetallah M, Ding M, Ke Z, Luo J (2007). The role of glycogen synthase kinase 3beta in the transformation of epidermal cells. Cancer Res 67, 7756–7764.

Mahanty S, Ravichandran K, Chitirala P, Prabha J, Jani RA, Setty SR (2016). Rab9A is required for delivery of cargo from recycling endosomes to melanosomes. Pigment Cell Melanoma Res 29, 43–59.

Malan D, Elischer A, Hesse M, Wickstrom SA, Fleischmann BK, Bloch W (2013). Deletion of integrin linked kinase in endothelial cells results in defective RTK signaling caused by caveolin 1 mislocalization. Development 140, 987–995.

Namekata K, Harada C, Guo X, Kimura A, Kittaka D, Watanabe H, Harada T (2012). Dock3 stimulates axonal outgrowth via GSK-3beta-mediated microtubule assembly. J Neurosci 32, 264–274.

O'Meara RW, Michalski JP, Anderson C, Bhanot K, Rippstein P, Kothary R (2013). Integrin-linked kinase regulates process extension in oligodendrocytes via control of actin cytoskeletal dynamics. J Neurosci 33, 9781–9793.

Pereira JA, Benninger Y, Baumann R, Goncalves AF, Ozcelik M, Thurnherr T, Tricaud N, Meijer D, Fassler R, Suter U, Relvas JB (2009). Integrin-linked kinase is required for radial sorting of axons and Schwann cell remyelination in the peripheral nervous system. J Cell Biol 185, 147–161.

Raposo G, Marks MS (2007). Melanosomes—dark organelles enlighten endosomal membrane transport. Nat Rev Mol Cell Biol 8, 786–797.

Risinger AL, Riffle SM, Lopus M, Jordan MA, Wilson L, Mooberry SL (2014). The taccalonolides and paclitaxel cause distinct effects on microtubule dynamics and aster formation. Mol Cancer 13, 41.

Robinson CL, Evans RD, Sivarasa K, Ramalho JS, Briggs DA, Hume AN (2019). The adaptor protein melanophilin regulates dynamic myosin–Va:cargo interaction and dendrite development in melanocytes. Mol Biol Cell 30, 742–752.

Rueden CT, Schindelin J, Hiner MC, DeZonia BE, Walter AE, Arena ET, Eliceiri KW (2017). ImageJ2: ImageJ for the next generation of scientific image data. BMC Bioinformatics 18, 529.

Sayedyahossein S, Xu SX, Rudkouskaya A, McGavin MJ, McCormick JK, Dagnino L (2015). *Staphylococcus aureus* keratinocyte invasion is mediated by integrin-linked kinase and Rac1. FASEB J 29, 711–723.
Schindelin J, Arganda-Carreras I, Frise E, Kaynig V, Longair M, Pietzsch T, Preibisch S, Rueden C, Saalfeld S, Schmid B, *et al*. (2012). Fiji: an open-source platform for biological-image analysis. Nat Methods 9, 676–682.
Sumi T, Imasaki T, Aoki M, Sakai N, Nitta E, Shirouzu M, Nitta R (2018). Structural insights into the altering function of CRMP2 by phosphorylation. Cell Struct Funct 43, 15–23.
Tadokoro R, Murai H, Sakai KI, Okui T, Yokota Y, Takahashi Y (2016). Melanosome transfer to keratinocyte in the chicken embryonic skin is mediated by vesicle release associated with Rho-regulated membrane blebbing. Sci Rep 6, 38277.
Tarafder AK, Bolasco G, Correia MS, Pereira FJ, Iannone L, Hume AN, Kirkpatrick N, Picardo M, Torrisi MR, Rodrigues IP, *et al*. (2014). Rab11b mediates melanin transfer between donor melanocytes and acceptor keratinocytes via coupled exo/endocytosis. J Invest Dermatol 134, 1056–1066.
Terpstra L, Prud'homme J, Arabian A, Takeda S, Karsenty G, Dedhar S, St-Arnaud R (2003). Reduced chondrocyte proliferation and chondrodysplasia in mice lacking the integrin-linked kinase in chondrocytes. J Cell Biol 162, 139–148.
Trinczek B, Ebneth A, Mandelkow EM, Mandelkow E (1999). Tau regulates the attachment/detachment but not the speed of motors in microtubule-dependent transport of single vesicles and organelles. J Cell Sci 112 (Pt 14), 2355–2367.
Van Gele M, Dynoodt P, Lambert J (2009). Griscelli syndrome: a model system to study vesicular trafficking. Pigment Cell Melanoma Res 22, 268–282.
Vaynberg J, Fukuda K, Lu F, Bialkowska K, Chen Y, Plow EF, Qin J (2018). Non-catalytic signaling by pseudokinase ILK for regulating cell adhesion. Nat Commun 9, 4465.
Vespa A, D'Souza SJ, Dagnino L (2005). A novel role for integrin-linked kinase in epithelial sheet morphogenesis. Mol Biol Cell 16, 4084–4095.
Watabe H, Valencia JC, Le Pape E, Yamaguchi Y, Nakamura M, Rouzaud F, Hoashi T, Kawa Y, Mizoguchi M, Hearing VJ (2008). Involvement of dynein and spectrin with early melanosome transport and melanosomal protein trafficking. J Invest Dermatol 128, 162–174.
Wickstrom SA, Lange A, Hess MW, Polleux J, Spatz JP, Kruger M, Pfaller K, Lambacher A, Bloch W, Mann M, *et al*. (2010). Integrin-linked kinase controls microtubule dynamics required for plasma membrane targeting of caveolae. Dev Cell 19, 574–588.
Wu X, Bowers B, Wei Q, Kocher B, Hammer JA 3rd (1997). Myosin V associates with melanosomes in mouse melanocytes: evidence that myosin V is an organelle motor. J Cell Sci 110 (Pt 7), 847–859.
Wu X, Hammer JA (2014). Melanosome transfer: it is best to give and receive. Curr Opin Cell Biol 29C, 1–7.
Yaar M, Park HY (2012). Melanocytes: a window into the nervous system. J Invest Dermatol 132, 835–845.
Yamaguchi Y, Hearing VJ (2014). Melanocytes and their diseases. Cold Spring Harb Perspect Med 4, a017046.
Yoshimura T, Kawano Y, Arimura N, Kawabata S, Kikuchi A, Kaibuchi K (2005). GSK-3beta regulates phosphorylation of CRMP-2 and neuronal polarity. Cell 120, 137–149.